Chapter 1

Fermi Theory of Beta Decay

> *"Fermi's theory of β decay is the prototype of all weak-interaction calculations: a contact coupling times phase space."*
>
> standard nuclear-physics assessment [6, 14]

Lecture 18 introduced the continuous β spectrum and Fermi's golden rule. This lecture completes the original course derivation: plane-wave leptons and the allowed approximation, phase-space counting for electron and neutrino (with explicit volume cancellation), conversion to the electron kinetic energy K with the *correct* momentum–energy factor structure, the Coulomb Fermi function $F(Z, K)$, Fermi–Kurie plots, and the classification of allowed Fermi and Gamow–Teller transitions versus forbidden decays. The algebra follows Krane and Dunlap [6, 1, 14, 2].

1.1 Matrix element and plane-wave leptons

The partial decay rate depends on the matrix element of the weak interaction H_{int} between initial and final states:

$$|M_{if}|^2 = |\langle \psi_{\text{d}}\, \psi_e\, \psi_\nu | H_{\text{int}} | \psi_{\text{p}} \rangle|^2 \,. \tag{1.1}$$

For β^- decay, ψ_{p} is the parent nucleus, ψ_{d} the daughter, and ψ_e, ψ_ν the electron and antineutrino.

Free leptons are modelled as plane waves normalised in a large volume V:

$$\psi_e(\boldsymbol{r}) = \frac{1}{\sqrt{V}} e^{i\boldsymbol{p}_e\cdot\boldsymbol{r}/\hbar}, \qquad \psi_\nu(\boldsymbol{r}) = \frac{1}{\sqrt{V}} e^{i\boldsymbol{p}_\nu\cdot\boldsymbol{r}/\hbar}. \tag{1.2}$$

Expanding the electron factor,

$$\frac{1}{\sqrt{V}} e^{i\boldsymbol{p}_e\cdot\boldsymbol{r}/\hbar} = \frac{1}{\sqrt{V}} \left(1 + \frac{i\boldsymbol{p}_e\cdot\boldsymbol{r}}{\hbar} + \frac{(i\boldsymbol{p}_e\cdot\boldsymbol{r})^2}{2!\,\hbar^2} + \cdots \right). \tag{1.3}$$

The **allowed approximation** keeps only the leading constant term, equivalent to evaluating the lepton wave function at the origin ($\boldsymbol{r} = \boldsymbol{0}$). This corresponds to orbital angular momentum $\ell = 0$ for the lepton pair. The nuclear matrix element

$$M_{if} = \int \psi_{\text{d}}^*(\boldsymbol{r})\, H_{\text{int}}\, \psi_{\text{p}}(\boldsymbol{r})\, \mathrm{d}^3 r \tag{1.4}$$

is then nearly constant over the β spectrum, and the energy dependence comes from phase space [6, 1].

Squaring the transition amplitude, each lepton contributes a factor $1/V$:

$$|\langle\psi_f|H_{\text{int}}|\psi_i\rangle|^2 = \frac{|M_{if}|^2}{V^2}. \tag{1.5}$$

This $1/V^2$ will cancel against the V^2 from lepton phase space (Section 1.2).

1.2 Phase-space density and volume cancellation

1.2.1 Single-particle density of states

Consider a free particle of momentum p confined to a cube of side L, volume $V = L^3$. Standing-wave quantisation gives momentum components $p_x = n_x\pi\hbar/L$ with positive integers n_x. The spacing in each direction is $\pi\hbar/L$, so the volume per quantum state in momentum space is $(\pi\hbar/L)^3 = h^3/V$.

The number of states with momentum magnitude between p and $p + \mathrm{d}p$ equals the number of lattice points in a spherical shell. Only the positive octant ($p_x, p_y, p_z > 0$) contributes, giving shell volume $\pi p^2 \mathrm{d}p/2$. Dividing by the volume per state,

$$\mathrm{d}n = \frac{\pi p^2\,\mathrm{d}p/2}{h^3/V} = \frac{4\pi p^2\,\mathrm{d}p\,V}{h^3}. \tag{1.6}$$

Equivalently, the uncertainty-principle argument assigns one state per cell $\Delta x\,\Delta y\,\Delta z\,\Delta p_x\,\Delta p_y\,\Delta p_z \sim h^3$ in phase space, yielding the same result [6, 1].

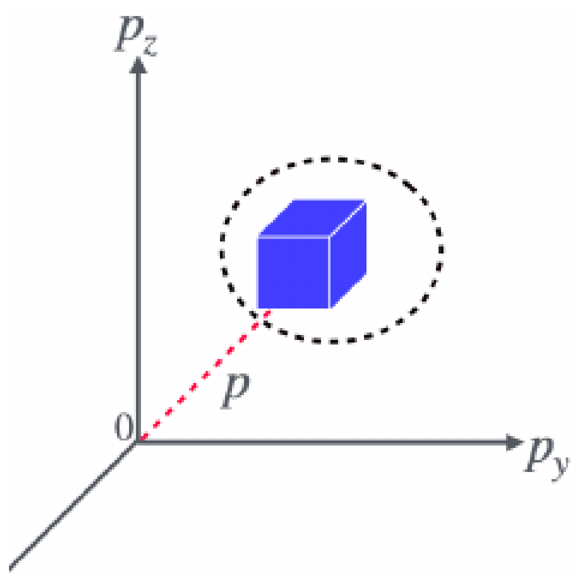

Figure 1.1: Momentum-space shell used to count lepton final states. Each quantum state occupies volume $\sim h^3/V$ in momentum space; the number of states in $\mathrm{d}p$ is $\mathrm{d}n = 4\pi p^2\,\mathrm{d}p\,V/h^3$.

1.2.2 Two leptons: product and cancellation

For β^- decay there are two free leptons. The combined number of final states in intervals $\mathrm{d}p_e$ and $\mathrm{d}p_\nu$ is the product:

$$\mathrm{d}n = \frac{4\pi p_e^2\,\mathrm{d}p_e\,V}{h^3}\cdot\frac{4\pi p_\nu^2\,\mathrm{d}p_\nu\,V}{h^3} = \frac{(4\pi)^2V^2}{h^6}\,p_e^2\,p_\nu^2\,\mathrm{d}p_e\,\mathrm{d}p_\nu. \tag{1.7}$$

From Fermi's golden rule (Lecture 18), the partial transition rate into this lepton momentum interval is

$$\mathrm{d}\lambda \propto \frac{|M_{if}|^2}{V^2}\cdot\frac{(4\pi)^2V^2}{h^6}\,p_e^2\,p_\nu^2\,\mathrm{d}p_e\,\mathrm{d}p_\nu = \frac{|M_{if}|^2}{h^6}\,p_e^2\,p_\nu^2\,\mathrm{d}p_e\,\mathrm{d}p_\nu. \tag{1.8}$$

The normalisation volume V cancels completely:

$$\frac{1}{V^2}\times V^2 = 1. \tag{1.9}$$

The decay rate is independent of the arbitrary box size and depends only on $|M_{if}|^2$ and lepton momenta [6, 1, 14].

1.3 Spectrum in kinetic energy: correct momentum–energy factors

We now express $\mathrm{d}\lambda$ in terms of electron kinetic energy K.

Energy conservation. Neglecting nuclear recoil and neutrino mass,

$$Q = K + E_\nu, \qquad p_\nu c = E_\nu = Q - K, \qquad p_\nu^2 = \frac{(Q-K)^2}{c^2}. \tag{1.10}$$

Relativistic electron kinematics. Total electron energy $E_e = K + m_ec^2$. The invariant relation $E_e^2 = p_e^2c^2 + m_e^2c^4$ gives

$$(K + m_ec^2)^2 = p_e^2c^2 + m_e^2c^4, \tag{1.11}$$

so

$$p_e^2 = \frac{K^2 + 2Km_ec^2}{c^2} = \frac{K(K+2m_ec^2)}{c^2}, \qquad p_e = \frac{\sqrt{K(K+2m_ec^2)}}{c}. \tag{1.12}$$

Differentiating p_e with respect to K. From $p_e^2c^2 = K^2 + 2Km_ec^2$, differentiate both sides:

$$2p_ec^2\,\mathrm{d}p_e = (2K + 2m_ec^2)\,\mathrm{d}K = 2(K + m_ec^2)\,\mathrm{d}K. \tag{1.13}$$

Hence

$$\mathrm{d}p_e = \frac{K + m_ec^2}{p_ec^2}\,\mathrm{d}K = \frac{K + m_ec^2}{\sqrt{K(K+2m_ec^2)}}\,\frac{\mathrm{d}K}{c}. \tag{1.14}$$

Neutrino phase-space factor at fixed K. At fixed electron kinetic energy K, the final-state energy constraint fixes p_ν. For a massless neutrino, $\mathrm{d}p_\nu/\mathrm{d}E_f = 1/c$, so the neutrino integration contributes a factor $1/c$ when converting to $\mathrm{d}K$.

Assembling the spectrum. The differential rate in $\mathrm{d}K$ is proportional to $p_e^2\,p_\nu^2\,\mathrm{d}p_e$. Substituting (1.11), (1.10), and (1.14):

$$\begin{aligned} p_e^2\,p_\nu^2\,\mathrm{d}p_e &\propto \frac{K(K+2m_ec^2)}{c^2}\cdot\frac{(Q-K)^2}{c^2}\cdot\frac{K+m_ec^2}{\sqrt{K(K+2m_ec^2)}}\,\frac{\mathrm{d}K}{c} \\ &= \frac{(K+m_ec^2)\,K(K+2m_ec^2)\,(Q-K)^2}{c^4\sqrt{K(K+2m_ec^2)}}\,\mathrm{d}K \\ &= \frac{\sqrt{K(K+2m_ec^2)}\,(K+m_ec^2)\,(Q-K)^2}{c^4}\,\mathrm{d}K. \end{aligned} \tag{1.15}$$

Absorbing c^4 and other constants into C, the **correct allowed spectrum** is

$$N(K)\,\mathrm{d}K = C\,|M_{if}|^2\,\underbrace{\sqrt{K(K+2m_ec^2)}}_{p_ec}\,\underbrace{(K+m_ec^2)}_{E_e}\,(Q-K)^2\,\mathrm{d}K. \tag{1.16}$$

Key idea

Correct factor structure (memorise this form).

$$N(K)\,\mathrm{d}K \propto p_e\,E_e\,(Q-K)^2\,\mathrm{d}K, \tag{1.17}$$
$$N(K) \propto \sqrt{K(K+2m_ec^2)}\,(K+m_ec^2)\,(Q-K)^2. \tag{1.18}$$

Here $p_ec = \sqrt{K(K+2m_ec^2)}$ and $E_e = K+m_ec^2$. The factor $(Q-K)^2$ comes from the neutrino phase space. This is *not* the same as $K\sqrt{K+2m_ec^2}\,(K+m_ec^2)(Q-K)^2$: the momentum factor is $p_ec = \sqrt{K(K+2m_ec^2)}$, not $K\sqrt{K+2m_ec^2}$. The erroneous extra factor $\sqrt{K}$ arises if one writes $p_e^2 \propto K(K+2m_ec^2)$ but replaces $p_e\,\mathrm{d}p_e$ inconsistently [6, 1].

Dunlap's equation (9.27) writes the same result as $(T_e^2+2T_em_ec^2)^{1/2}(Q-T_e)^2(T_e+m_ec^2)$, which is identical to (1.18) with $T_e = K$ [1, 6].

Momentum form. In terms of electron momentum p_e, with $K = (p_ec)^2/(2m_ec^2)$ in the ultrarelativistic limit but more generally from (1.12),

$$N(p_e)\,\mathrm{d}p_e \propto p_e^2\,(Q-K)^2\,\mathrm{d}p_e, \qquad K = K(p_e). \tag{1.19}$$

Both (1.17) and (1.18) must be used consistently when changing variables.

1.4 Fermi function $F(Z,K)$

The plane-wave approximation ignores the Coulomb interaction between the emitted β particle and the daughter nucleus of charge $+Ze$. For β^- decay the interaction is attractive; for β^+ it is repulsive. Quantum mechanically, this modifies the electron/positron wave function near the nucleus and multiplies the spectrum by the **Fermi function**

$$F(Z,K) = \frac{2\pi\eta}{1-e^{-2\pi\eta}}, \tag{1.20}$$

with

$$\eta = \pm \frac{Ze^2}{4\pi\varepsilon_0\,\hbar v}. \tag{1.21}$$

The plus sign applies to β^- (electron attracted); the minus sign to β^+ (positron repelled). Here Z is the *daughter* atomic number and v is the lepton speed [6, 1].

Relativistic velocity. The relativistic relation is

$$v = \frac{p_e c^2}{E_e} = \frac{\sqrt{K(K + 2m_e c^2)}}{K + m_e c^2}\, c. \tag{1.22}$$

A *non-relativistic* estimate $v \approx \sqrt{2K/m_e}$ is sometimes used for low K, but MeV-scale β particles require (1.22) [6, 1, 14].

Using $e^2/(4\pi\varepsilon_0) = \hbar c/137 \approx 1.44\,\text{MeV fm}$ and $\hbar c \approx 197\,\text{MeV fm}$,

$$\eta = \pm \frac{Z \times 1.44\,\text{MeV fm}\, c}{197\,\text{MeV fm}\, v} = \pm \frac{Z \times 1.44}{197}\,\frac{c}{v}. \tag{1.23}$$

The full spectrum including Coulomb corrections is

$$N(K)\,\mathrm{d}K \propto F(Z,K)\,\sqrt{K(K + 2m_e c^2)}\,(K + m_e c^2)\,(Q - K)^2\,\mathrm{d}K. \tag{1.24}$$

$F > 1$ enhances low-energy β^- electrons and suppresses low-energy positrons, explaining why the ^{64}Cu β^- and β^+ spectra in Lecture 18 differ in shape even though the bare phase space (1.16) is the same [1, 6].

Remark

The Fermi function (1.20) is most important at low K, where v is small and η is large. At high K the Coulomb correction approaches unity. Fully relativistic Coulomb wave functions (Fermi–Longmire) are used in precision work [6, 1].

1.5 Fermi–Kurie plot

To test (1.24) against data, one linearises the spectrum. From (1.19) and (1.24), the momentum-space intensity is

$$I(p_e) \propto p_e^2\,(Q - K)^2\,F(Z,K). \tag{1.25}$$

Therefore

$$\sqrt{\frac{N(p_e)}{p_e^2\,F(Z,K)}} \propto (Q - K). \tag{1.26}$$

A plot of $\sqrt{N/(p^2F)}$ versus K (or total electron energy) is a **Fermi–Kurie plot**. For allowed transitions with constant $|M_{if}|^2$, the plot is a straight line intercepting $K = Q$ at zero intensity [6, 1].

^{66}Ga: allowed benchmark. $^{66}\text{Ga}(0^+) \to {}^{66}\text{Zn}(0^+) + \beta^+ + \nu_e$: $\Delta I = 0$, no parity change, $\ell = 0$ lepton pair. The Kurie plot (Fig. 1.2) is linear, confirming the phase-space factor (1.18) and constant $|M_{if}|^2$ [6].

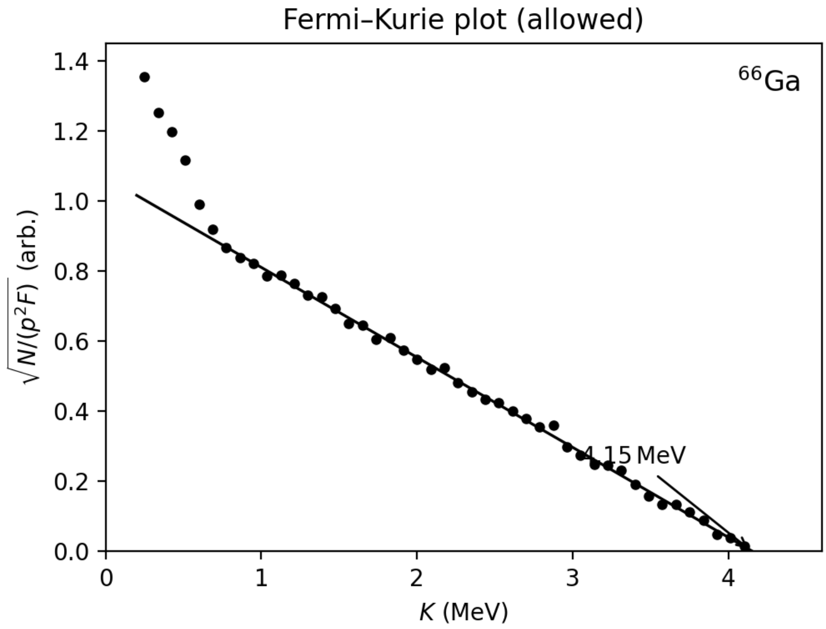

Figure 1.2: Fermi–Kurie plot for $^{66}\mathrm{Ga} \xrightarrow{\beta^+} {}^{66}\mathrm{Zn}$: allowed $0^+ \to 0^+$ transition. The plot of $\sqrt{N/(p^2F)}$ versus kinetic energy K is linear except at low energy (source scattering). Schematic reconstruction of the shape reported by Camp and Langer [31]; see also [6, 1].

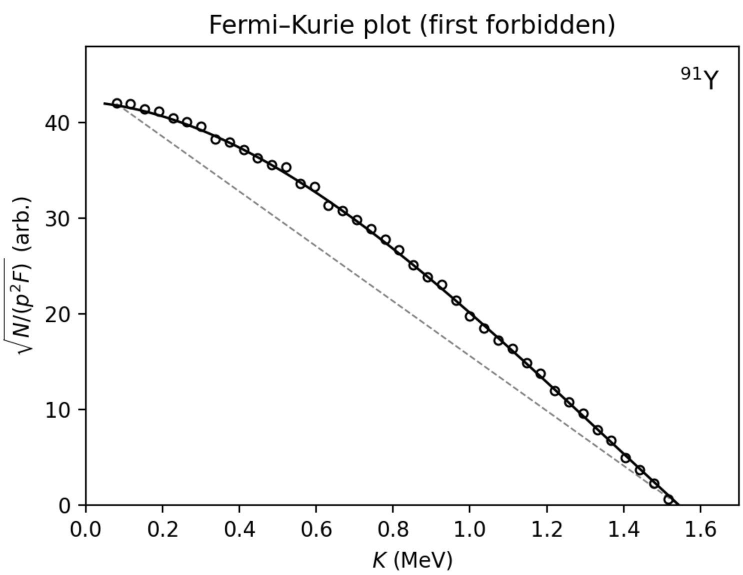

Figure 1.3: Fermi–Kurie plot for $^{91}\mathrm{Y} \xrightarrow{\beta^-} {}^{91}\mathrm{Zr}$: first-forbidden transition. The curve is convex (non-linear) relative to the dashed allowed line, indicating a non-constant shape factor. Schematic reconstruction of the shape reported by Langer and Price [30]; see also [6, 1].

^{91}Y: forbidden example. $^{91}\mathrm{Y}(\frac{1}{2}^-) \to {}^{91}\mathrm{Zr}(\frac{5}{2}^+) + e^- + \bar{\nu}_e$: $|\Delta I| = 2$ with parity change. The lepton pair must carry angular momentum; the $\ell = 0$ approximation fails. The Kurie plot (Fig. 1.3) bends upward (convex): a shape factor $S(K)$ multiplies the allowed spectrum [6, 1].

1.6 Allowed Fermi and Gamow–Teller transitions

The lepton wave function expansion (1.2) links orbital angular momentum to the power of $\boldsymbol{p}\cdot\boldsymbol{r}/\hbar$. Keeping only the constant term is the *allowed* ($\ell = 0$) approximation.

Electron and neutrino each have spin $s = \frac{1}{2}$. The total leptonic spin can be

$$S = 0 \quad \text{(singlet, spins antiparallel)} \qquad \text{or} \qquad S = 1 \quad \text{(triplet, spins parallel)}. \tag{1.27}$$

With $\ell = 0$, the total leptonic angular momentum is $J = \ell + S = S$.

Fermi (vector) transitions. $S = 0$, $J = 0$. Selection rules:

$$\Delta I = 0, \qquad \Delta\pi = 0 \quad \text{(no parity change)}. \tag{1.28}$$

Pure Fermi includes $0^+ \to 0^+$. The weak operator is approximately $\tau_\pm$ (isospin raising/lowering) acting on nucleons [6, 14].

Gamow–Teller (axial) transitions. $S = 1$, $J = 1$. Selection rules:

$$\Delta I = 0,\ \pm 1 \quad (\text{but not } 0^+ \to 0^+), \qquad \Delta\pi = 0. \tag{1.29}$$

The operator structure involves $\boldsymbol{\tau}_\pm\boldsymbol{\sigma}$ (isospin times nucleon spin) [6, 14, 2].

Key idea

Allowed ($\ell = 0$): Fermi ($S = 0$, $\Delta I = 0$, no parity change) vs Gamow–Teller ($S = 1$, $\Delta I = 0, \pm 1$, not $0 \to 0$, no parity change). Both use the spectrum (1.18); the difference is in $|M_{if}|^2$, not in the leading phase space.

1.7 Forbidden transitions, shape factors, and ft values

If $\ell = 0$ transitions are suppressed by angular momentum or parity selection rules, the next term in the plane-wave expansion ($\boldsymbol{p}\cdot\boldsymbol{r}/\hbar$) contributes. Transitions with leptonic orbital angular momentum $\ell \geq 1$ are called **forbidden**; the rate decreases rapidly as ℓ increases.

Order of forbiddenness. $\ell = 1$: first forbidden; $\ell = 2$: second forbidden; and so on [6, 1].

First-forbidden selection rules (summary). For $\ell = 1$, parity changes: $\Delta\pi = (-1)^\ell = -1$.

- First-forbidden Fermi ($\ell = 1$, $S = 0$): $\Delta I = 0, \pm 1$, $\Delta\pi = -1$.
- First-forbidden Gamow–Teller ($\ell = 1$, $S = 1$): $\Delta I = 0, \pm 1, \pm 2$, $\Delta\pi = -1$.

The ^{91}Y decay in Fig. 1.3 is first forbidden [6, 1].

Shape factor. Forbidden transitions multiply the allowed spectrum by an energy-dependent **shape factor** $S(K)$:

$$N(K)\,\mathrm{d}K = S(K)\,N_0(K)\,\mathrm{d}K, \tag{1.30}$$

where $N_0(K)\,\mathrm{d}K$ is the allowed form (1.24). When $S(K)$ is accounted for, the Kurie plot can be straightened [6, 1].

Comparative half-life ft. The partial half-life $t_{1/2}$ depends on $|M_{if}|^2$ and phase space. The **comparative half-life**

$$ft = \frac{\ln 2}{|M_{if}|^2\, f(Z,Q)} \tag{1.31}$$

removes the phase-space integral $f(Z,Q)$, leaving a quantity determined by nuclear structure alone. Values of $\log_{10} ft$ classify transitions:

$\log_{10} ft$	Classification
3–3.5	Superallowed Fermi
~ 5	Allowed
6–10	First forbidden
> 10	Higher forbidden

Superallowed $0^+ \to 0^+$ Fermi decays determine the vector coupling G_V and, combined with muon decay, the CKM element V_{ud} [6, 1, 20].

Caution

"Forbidden" does not mean impossible: ^{91}Y β-decays with $t_{1/2} \approx 58\,$d. It means the transition is suppressed relative to allowed decays with similar Q [6].

Key idea

Students should remember:

- Phase space: $\mathrm{d}n = 4\pi p^2\,\mathrm{d}p\,V/h^3$; two leptons give $p_e^2 p_\nu^2$; V^2 cancels $1/V^2$ from $|M|^2$.
- Correct spectrum: $N(K) \propto p_e E_e (Q-K)^2$, equivalently $\sqrt{K(K+2m_ec^2)}(K+m_ec^2)(Q-K)^2$.
- Fermi function: $F = 2\pi\eta/(1-e^{-2\pi\eta})$, $\eta = \pm Ze^2/(4\pi\varepsilon_0\hbar v)$, $v = p_ec^2/E_e$.
- Kurie plot: $\sqrt{N/(p^2F)}$ vs K linear for allowed decays.
- Fermi: $S=0$, $\Delta I = 0$; GT: $S=1$, $\Delta I = 0,\pm 1$, not $0 \to 0$; forbidden: $\ell \geq 1$, shape factor $S(K)$.

1.8 Further physics from the literature

Neutrino mass and the endpoint. All expressions above assume $m_\nu = 0$, so $p_\nu c = E_\nu = Q - K$ and $(Q-K)^2$ appears in the spectrum. If $m_\nu \neq 0$, near the endpoint ($K \to Q$) the neutrino becomes non-relativistic and $p_\nu = \sqrt{2m_\nu(Q-K)}$. The phase-space factor $(Q-K)^2$

is replaced by $2m_\nu(Q-K)$, and the slope of $N(K)$ at $K=Q$ changes from zero ($m_\nu = 0$, tangential approach) to infinite ($m_\nu \neq 0$, perpendicular approach). Precision β-spectroscopy near the tritium endpoint constrains m_{ν_e} [6, 14, 2].

Comparative half-lives and weak coupling. The product ft in (1.31) removes the calculated phase-space integral $f(Z,Q)$ so that $\log_{10} ft$ reflects only nuclear matrix elements. Superallowed $0^+ \to 0^+$ Fermi transitions (for example ^{14}O, ^{10}C) give the most precise value of G_V. Combined with muon decay, this determines the Cabibbo angle and V_{ud} in the quark mixing matrix [6, 1, 20].

From Fermi contact to W boson. Fermi's 1934 point interaction is the low-energy limit of charged-current exchange mediated by $W^\pm$ bosons ($m_W \approx 80\,\mathrm{GeV}/c^2$). At nuclear β energies the propagator momentum is so large that the interaction looks local, with strength set by G_F [14, 5, 2].

Experimental databases. Half-lives, Q-values, and branching ratios used in problems are tabulated in ENSDF and NuDat 3 [20, 21]. Kurie-plot data for ^{64}Cu, ^{66}Ga, and ^{91}Y appear in the classic papers by Langer *et al.* (1949) and Camp and Langer (1963), reproduced in Krane and Dunlap [6, 1].

From the literature

Basdevant *et al.* emphasise that the β spectrum is the earliest example of a three-body decay treated with relativistic phase space; the same methods reappear in muon and heavy-lepton decays [14]. Demtröder discusses modern tritium experiments and the KATRIN limit on m_{ν_e} [2].

Applications. The β spectrum shape enters dosimetry (medical isotopes), reactor antineutrino flux calculations, and detector calibration. NMR spin polarisation relies on β–γ angular correlations in allowed decays [13, 6].

1.9 Problems with solutions

Problem 19.1 — Derive the spectrum from phase space

Starting from $\mathrm{d}\lambda \propto p_e^2 p_\nu^2\,\mathrm{d}p_e$ with $p_\nu c = Q-K$ and relativistic electron kinematics, derive

$$N(K)\,\mathrm{d}K \propto \sqrt{K(K+2m_ec^2)}\,(K+m_ec^2)\,(Q-K)^2\,\mathrm{d}K. \tag{1.32}$$

Show every algebraic step [1, 6].

Step-by-step

Step 1: Neutrino factor. $p_\nu c = E_\nu = Q-K$, so $p_\nu^2 = (Q-K)^2/c^2$.

Step 2: Electron momentum squared. From $E_e = K + m_e c^2$ and $E_e^2 = p_e^2 c^2 + m_e^2 c^4$:

$$p_e^2 c^2 = K^2 + 2K m_e c^2 \quad \Rightarrow \quad p_e^2 = \frac{K(K + 2m_e c^2)}{c^2}.$$

Step 3: Differentiate for $\mathrm{d}p_e$. From $p_e^2 c^2 = K^2 + 2K m_e c^2$:

$$2p_e c^2 \, \mathrm{d}p_e = 2(K + m_e c^2) \, \mathrm{d}K \quad \Rightarrow \quad \mathrm{d}p_e = \frac{K + m_e c^2}{p_e c^2} \, \mathrm{d}K.$$

Step 4: Assemble.

$$p_e^2 p_\nu^2 \, \mathrm{d}p_e = \frac{K(K + 2m_e c^2)}{c^2} \cdot \frac{(Q - K)^2}{c^2} \cdot \frac{K + m_e c^2}{p_e c^2} \, \mathrm{d}K.$$

Step 5: Substitute p_e. Use $p_e = \sqrt{K(K + 2m_e c^2)}/c$:

$$p_e^2 p_\nu^2 \, \mathrm{d}p_e = \frac{K(K + 2m_e c^2)(Q - K)^2}{c^4} \cdot \frac{K + m_e c^2}{\sqrt{K(K + 2m_e c^2)}} \, \mathrm{d}K.$$

Step 6: Simplify. Cancel one factor $\sqrt{K(K + 2m_e c^2)}$ from numerator and denominator:

$$p_e^2 p_\nu^2 \, \mathrm{d}p_e = \frac{\sqrt{K(K + 2m_e c^2)} \, (K + m_e c^2) \, (Q - K)^2}{c^4} \, \mathrm{d}K.$$

Step 7: Identify $p_e c$ and E_e.

$$\sqrt{K(K + 2m_e c^2)} = p_e c, \qquad K + m_e c^2 = E_e,$$

so $N(K) \, \mathrm{d}K \propto p_e E_e (Q - K)^2 \, \mathrm{d}K$, as required [1, 6].

Problem 19.2 — Endpoint and maximum of $N(K)$

For allowed β^- decay with $Q = 1.0\,\mathrm{MeV}$ and $m_e c^2 = 0.511\,\mathrm{MeV}$, show that $N(K) = 0$ at $K = Q$ and estimate $K_{\max}$ where $N(K)$ peaks (numerically or graphically).

Step-by-step

At $K = Q$: the factor $(Q - K)^2 = 0$, so $N(Q) = 0$. This is the spectrum endpoint.
For the maximum, set $dN/dK = 0$ on the allowed form (ignoring F):

$$N(K) \propto \sqrt{K(K + 2m_e c^2)} \, (K + m_e c^2) \, (Q - K)^2.$$

At $Q = 1.0\,\mathrm{MeV}$, plotting or numerical differentiation gives $K_{\max} \approx 0.58$–$0.60\,\mathrm{MeV}$: the spectrum peaks well below Q because the $(Q - K)^2$ factor favours sharing energy with the neutrino [6, 1].

Problem 19.3 — Fermi parameter η

For β^- decay to a daughter with $Z = 30$, find η and comment on $F(Z, K)$ at $K = 0.10\,\text{MeV}$ and $K = 1.0\,\text{MeV}$. Use $v = p_e c^2/E_e$.

Step-by-step

At $K = 0.10\,\text{MeV}$:

$$p_e c = \sqrt{0.10 \times 1.122} = 0.335\,\text{MeV}, \quad E_e = 0.611\,\text{MeV},$$

$$v = \frac{p_e c^2}{E_e} = 0.548c, \qquad \eta = +\frac{30 \times 1.44}{197 \times 0.548} \approx 0.40.$$

Then $F = 2\pi\eta/(1 - e^{-2\pi\eta}) \approx 2.5$: Coulomb enhancement is large.

At $K = 1.0\,\text{MeV}$: $p_e c = 1.22\,\text{MeV}$, $E_e = 1.511\,\text{MeV}$, $v = 0.807c$, $\eta \approx 0.27$, $F \approx 1.8$. Enhancement decreases at higher K [6, 1].

Problem 19.4 — Kurie plot intercept

A Fermi–Kurie plot of $\sqrt{N/(p^2F)}$ versus K for an allowed β^- decay is a straight line with slope $-0.50\,\text{MeV}^{-1}$ and intercept at $K = 2.50\,\text{MeV}$ on the horizontal axis. What is Q?

Step-by-step

For allowed decays, $\sqrt{N/(p^2F)} \propto (Q - K)$. The intercept where intensity vanishes is $K = Q$. Therefore $Q = 2.50\,\text{MeV}$ [6, 1].

Problem 19.5 — Classify ^{66}Ga and ^{91}Y

State whether each decay is allowed or forbidden, Fermi or Gamow–Teller, and predict the Kurie-plot shape.

Step-by-step

$^{66}\text{Ga}(0^+) \to {}^{66}\text{Zn}(0^+)$: $\Delta I = 0$, $\Delta\pi = 0$, $\ell = 0$. Allowed Fermi. Kurie plot linear (Fig. 1.2) [6].

$^{91}\text{Y}(\frac{1}{2}^-) \to {}^{91}\text{Zr}(\frac{5}{2}^+)$: $|\Delta I| = 2$, parity changes. First forbidden (minimum $\ell = 1$). Kurie plot non-linear, convex (Fig. 1.3) [6, 1].

Problem 19.6 — Common error check

A student writes $N(K) \propto K\sqrt{K + 2m_ec^2}(K + m_ec^2)(Q - K)^2$. Explain why this differs from the correct formula and identify the extra factor.

Step-by-step

The correct momentum factor is $p_e c = \sqrt{K(K + 2m_e c^2)}$, not $K\sqrt{K + 2m_e c^2}$. The student expression has an extra factor of $\sqrt{K}$ relative to the correct form $\sqrt{K(K + 2m_e c^2)}(K + m_e c^2)(Q - K)^2$. This error typically arises from using $p_e^2 \propto K(K + 2m_e c^2)$ but failing to include the $\mathrm{d}p_e$ Jacobian correctly, or from confusing $p_e c$ with $K\sqrt{K + 2m_e c^2}$ [1, 6].

Bibliography

[1] R. A. Dunlap, *An Introduction to the Physics of Nuclei and Particles* (2nd ed.), IOP Publishing, Bristol (2023), DOI: 10.1088/978-0-7503-6094-4, Ch. 3 (Nuclear composition and size).

[2] W. Demtröder, *Nuclear and Particle Physics*, Undergraduate Lecture Notes in Physics, Springer, Cham (2023).

[3] S. Petrera, *Problems and Solutions in Nuclear and Particle Physics*, UNITEXT for Physics, Springer, Cham (2019).

[4] F. Terranova, *A Modern Primer in Particle and Nuclear Physics*, Oxford University Press (2021).

[5] S. D'Auria, *Introduction to Nuclear and Particle Physics*, Undergraduate Lecture Notes in Physics, Springer, Cham (2018).

[6] K. S. Krane, *Introductory Nuclear Physics*, Wiley, New York (1988).

[7] R. Hofstadter, "Electron scattering and nuclear structure," Rev. Mod. Phys. **28**, 214 (1956).

[8] H. F. Ehrenberg, R. Hofstadter, U. Meyer-Berkhout, D. G. Ravenhall, and S. E. Sobottka, "High-Energy Electron Scattering and the Charge Distribution of Carbon-12 and Oxygen-16," Phys. Rev. **113**, 666 (1959).

[9] H. Yukawa, "On the interaction of elementary particles. I," Proc. Phys.-Math. Soc. Japan **17**, 48 (1935).

[10] R. D. Woods and D. S. Saxon, "Diffuse surface optical model for nucleon-nuclei scattering," Phys. Rev. **95**, 577 (1954).

[11] H. G. J. Moseley, "The high-frequency spectra of the elements," Phil. Mag. **26**, 1024 (1913); **27**, 703 (1914).

[12] C. F. von Weizsäcker, "Zur Theorie der Kernmassen," Z. Phys. **96**, 431 (1935).

[13] P. Cappellaro, *Introduction to Applied Nuclear Physics* (MIT OpenCourseWare / LibreTexts), CC BY-NC-SA 4.0.

[14] J.-L. Basdevant, J. Rich, and M. Spiro, *Fundamentals in Nuclear Physics: From Nuclear Structure to Cosmology*, Springer, New York (2005).

[15] D. Tong, *Particle Physics*, Lecture notes (University of Cambridge / CERN school notes).

[16] M. G. Mayer, "On closed shells in nuclei. II," Phys. Rev. **75**, 1969 (1949).

[17] O. Haxel, J. H. D. Jensen, and H. E. Suess, "On the "magic numbers" in nuclear structure," Phys. Rev. **75**, 1766 (1949).

[18] T. Schmidt, "Über die magnetischen Momente der Atomkerne," Z. Phys. **106**, 358 (1937).

[19] L. W. Nordheim, "On spins, moments, and shells in nuclei," Phys. Rev. **78**, 294 (1950).

[20] Evaluated Nuclear Structure Data File (ENSDF), National Nuclear Data Center, Brookhaven National Laboratory, `https://www.nndc.bnl.gov/ensdf/`.

[21] NuDat 3, National Nuclear Data Center, Brookhaven National Laboratory, `https://www.nndc.bnl.gov/nudat3/`.

[22] N. J. Stone, "Table of nuclear magnetic dipole and electric quadrupole moments," At. Data Nucl. Data Tables **90**, 75 (2005); updated compilations at NNDC.

[23] W. N. Cottingham and D. A. Greenwood, *An Introduction to Nuclear Physics* (2nd ed.), Cambridge University Press, Cambridge (2001).

[24] H. Geiger and J. M. Nuttall, "The ranges of the α particles from the radioactive substances," Phil. Mag. **22**, 613 (1911).

[25] G. Gamow, "Zur Quantentheorie des Atomkernes," Z. Phys. **51**, 204 (1928).

[26] R. W. Gurney and E. U. Condon, "Wave mechanics and radioactive disintegration," Nature **122**, 439 (1928); Phys. Rev. **33**, 127 (1929).

[27] M. Wang, W. J. Huang, F. G. Kondev, G. Audi, and S. Naimi, "The AME 2020 atomic mass evaluation (II). Tables, graphs and references," Chin. Phys. C **45**, 030003 (2021).

[28] Laboratoire National Henri Becquerel (LNHB), Recommended decay data, `http://www.lnhb.fr/nuclear-data/nuclear-data-table/`.

[29] L. M. Langer, R. D. Moffat, and H. C. Price, Jr., "Low energy beta-ray spectra: P^{32} and Cu^{64}," Phys. Rev. **76**, 1725 (1949).

[30] L. M. Langer and H. C. Price, Jr., "Shapes of the beta-spectra of the forbidden transitions of Sb^{124}, Rb^{86}, Sr^{89}, Y^{91}, and Cs^{137}," Phys. Rev. **75**, 1769 (1949).

[31] D. C. Camp and L. M. Langer, "The shape of the ^{66}Ga positron spectrum and the contribution from $0^+ \to 0^+$ transitions," Phys. Rev. **129**, 1782 (1963).